

Document downloaded from:

<http://hdl.handle.net/10251/120369>

This paper must be cited as:

Baselga Moreno, S. (2018). Fibonacci lattices for the evaluation and optimization of map projections. *Computers & Geosciences*. 117:1-8.
<https://doi.org/10.1016/j.cageo.2018.04.012>



The final publication is available at

<http://doi.org/10.1016/j.cageo.2018.04.012>

Copyright Elsevier

Additional Information

Fibonacci lattices for the evaluation and optimization of map projections

Sergio Baselga

Cartographic Engineering, Geodesy and Photogrammetry Dept., Universitat Politècnica de València, Camino de Vera s/n, 46022 Valencia, Spain. E-mail address: serbamo@cgf.upv.es

ABSTRACT

Latitude-longitude grids are frequently used in geosciences for global numerical modelling although they are remarkably inhomogeneous due to meridian convergence. In contrast, Fibonacci lattices are highly isotropic and homogeneous so that the area represented by each lattice point is virtually the same. In the present paper we show the higher performance of Fibonacci versus latitude-longitude lattices for evaluating distortion coefficients of map projections. In particular, we obtain first a typical distortion for the Lambert Conformal Conic projection with their currently defined parameters and geographic boundaries for Europe that has been adopted as standard by the INSPIRE directive. Further, we optimize the defining parameters of this projection, lower and upper standard parallel latitudes, so that the typical distortion for Europe is reduced a 10% when they are set to 36° and 61.5° , respectively. We also apply the optimization procedure to the determination of the best standard parallels for using this projection in Spain, whose values remained unspecified by the National decree that commanded its official adoption, and obtain optimum values of 37° and 42° and a resulting typical distortion of 828 ppm.

Keywords: Fibonacci lattices; Lambert Conformal Conic projection; standard parallels; optimization.

1. Introduction

The effective evaluation of scalar models for a particular area is an issue frequently encountered in geosciences. The standard approach is to use regular latitude-longitude lattices, which are conceptually simple and generally easy to implement in any software. They suffer, however, from fundamental problems especially associated with the meridian convergence, which often make them ineffective for the evaluation of the model in the geographic area under study.

In the last decades, some alternatives to latitude-longitude lattices have been proposed for global numerical modelling, which have some desirable properties such as higher geometrical regularity and isotropic spatial resolution as well as ease of parallelization (Purser 1999). They generally require a lower number of lattice points than standard latitude-longitude lattices to obtain results of the same quality. Among them, Fibonacci lattices have emerged as powerful tools to enhance numerical effectiveness due to their virtual uniformity and isotropic resolution (Swinbank and Purser, 2006).

While the regular hexagonal lattice provides optimal sampling for the plane (Conway and Sloane, 1998), it is impossible to arrange regularly more than 20 points on the sphere let alone on the ellipsoid. The usual latitude-longitude lattice is highly inhomogeneous and far from the desired situation where every point represents almost the same area, which can be virtually obtained with the use of a Fibonacci lattice, a mathematical idealization of natural patterns with optimal packing. González (2010) takes advantage of this feature and applies Fibonacci lattices to the problem of area determination by means of point counting, obtaining results with at least 40% error reduction when compared to the use of latitude-longitude lattices. Other applications of Fibonacci lattices can be found in disparate fields as shallow water modelling, climate models and three-dimensional numerical weather prediction (Swinbank and Purser, 2006) including tornado outbreak prediction (Sparrow and Mercer, 2016), air traffic networks (Monechi *et al.* 2015), electron paramagnetic

52 resonance (Crăciun, 2014) and approximation of spherical integrals for image sampling (Marques
53 *et al.* 2013).

54
55 In the present paper we propose to apply Fibonacci lattices first as a tool to evaluate map projection
56 distortions and then to optimize their defining parameters so that the resulting map projection has
57 minimum distortion for a particular area of use. More specifically, starting from Airy (1861) and
58 Jordan (1896)'s measures of distortion, we will define an optimization function based on the square
59 mean deviation from unity of the scale distortion coefficient of a conformal map projection over a
60 representative Fibonacci lattice of the area under study and compute its optimum. Since Conic Map
61 projections are suitable for mid-latitude regions with predominant East-West extension (Snyder,
62 1987; Savric and Jenny, 2016), they have often been required or recommended by national
63 mapping agencies or international consortiums. In particular, the Lambert Conformal Conic
64 projection was proposed, first, by EuroGeographics, the consortium of European national mapping,
65 cadastral and land registry authorities (Annoni *et al.*, 2003) for conformal representations of
66 Europe, and then adopted by INSPIRE D2.8.I.1 (2014), the European Commission directive for
67 spatial information, as the standard for conformal mapping in Europe. We want now to evaluate the
68 distortions this projection introduces, first, and then investigate whether the definition of other
69 standard parallels than the two recommended by EuroGeographics and then adopted by INSPIRE,
70 produces significantly better results. As an additional example, we will also apply our methods to
71 the particular case of Spain, where the Lambert Conformal Conic projection has been officially
72 adopted for land representation at mapping scales of 1:500.000 or lower (Gobierno del Estado
73 Español, 2007). This decree does not fix, however, the standard parallel latitudes to be used, so we
74 will compute the ones that minimize the resulting distortions by means of our method based on
75 Fibonacci lattices.

76 2. Methods

77 2.1. Latitude-longitude lattices

78
79 For a given geographic domain, a latitude-longitude lattice is easily constructed after the definition
80 of a grid step δ so that points are generated for all pairs that can be formed with $(\varphi_{min}, \varphi_{min} + \delta, \varphi_{min}$
81 $+ 2\delta, \dots)$ (all latitudes lower than the maximum possible latitude) and $(\lambda_{min}, \lambda_{min} + \delta, \lambda_{min} + 2\delta, \dots)$
82 (all longitudes lower than the maximum possible longitude). Due to the meridian convergence the
83 distribution of points is denser in polar areas, which makes the lattice remarkably inhomogeneous.
84

85 When we use latitude-longitude lattices we normally need a considerably large number of sampling
86 points in the area (small step size δ) to obtain a stable value that does not depend significantly on
87 the number of sampling points. Even then the value may oscillate a bit. We can improve the
88 performance of latitude-longitude lattices by using a weighting function so that the abundance of
89 points at higher latitudes is compensated by a lower weight in the computation. Following
90 González (2010) in order to compensate for higher density at higher latitudes we must use for every
91 lattice point i the weight function

$$92 \quad 93 \quad w_i = \cos\varphi_i \quad (1)$$

Código de campo cambiado

96 2.2. Fibonacci lattices

97
98 Contrary to latitude-longitude lattices, a Fibonacci lattice has the property of regular isotropic
99 distribution. It bears its name from Leonardo Pisano, alias Fibonacci, a medieval mathematician
100 who discovered the sequence 0, 1, 1, 2, 3, 5, 8, 13, 21... in which every number (starting from the
101 third) is the sum of the previous two. This series, initially developed by Fibonacci to account for
102 the population of rabbit breeding in the different generations, appears in many biological systems
103 (such as branching and arrangement of leaves in plants and trees, petal flowering, beehives, etc.) as
104 well as in chemical composition of materials, music theory and other apparently detached areas

105 such as economic theory (see e.g. Koshy, 2001). As the series progresses to infinity, the ratio
 106 between consecutive numbers, F_i and F_{i+1} , approaches the so-called golden ratio Φ
 107

$$108 \quad \lim_{i \rightarrow \infty} \frac{F_{i+1}}{F_i} = \Phi \quad (2)$$

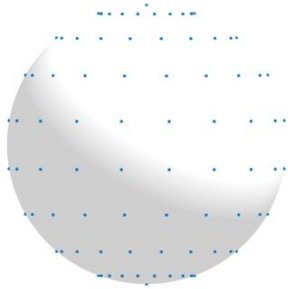
109
 110 This golden ratio is the number whose inverse is the number itself minus one
 111
 112

$$113 \quad \Phi = 1 + \frac{1}{\Phi} = \frac{1 + \sqrt{5}}{2} \approx 1.61803399 \quad (3)$$

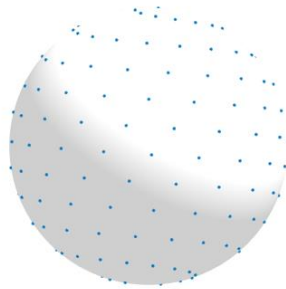
114 The Fibonacci lattice is generated by a spiral with evenly spaced points, being the longitudinal turn
 115 between consecutive points defined by $360^\circ \Phi^{-1} \approx 222.5^\circ$ or by its complement to 360° , i.e. $360^\circ(1 -$
 116 $\Phi^{-1}) = 360^\circ \Phi^{-2} \approx 137.5^\circ$. Following González (2010) we generate a Fibonacci lattice with
 117 longitudinal turns between consecutive points of $360^\circ \Phi^{-1}$, if, given a natural number N , we compute
 118 the set of geographic coordinates for points $i = -N, -N + 1, \dots, 0, N - 1, N$ as
 119

$$121 \quad \begin{aligned} \varphi_i &= \arcsin\left(\frac{2i}{2N+1}\right) \times \frac{180^\circ}{\pi} & i &= -N, -N + 1, \dots, 0, N - 1, N \\ \lambda_i &= 360^\circ \Phi^{-1} i = 360^\circ \times \text{mod}(i, \Phi) / \Phi \end{aligned} \quad (4)$$

122 The function $\text{mod}(i, \Phi)$ returns the remainder of the division of i by Φ , eliminating thus the
 123 unnecessary turns of the spiral (i.e. additive values of 360° for each spiral turn). The geographic
 124 coordinates φ_i, λ_i that are obtained by means of Eq. (4) for every point i of the lattice are given in
 125 degrees. This results in $2N+1$ total points for the lattice, being each of them located in a different
 126 latitude, which provides a much more homogeneous sampling than the case of the latitude-
 127 longitude lattice. Just for the purpose of illustration we depict in Fig. 1 the results of a latitude-
 128 longitude lattice over a sphere with 180 points ($\delta = 20^\circ$) and in Fig. 2 the results of a Fibonacci
 129 lattice over a sphere with 179 points (Fibonacci lattices always have an odd number of points).
 130 While in Fig. 1 a high point density in polar areas contrasts with a quite sparse distribution of
 131 points near the equator, in Fig. 2 we have a much more uniform point density.
 132



133
 134
 135
 136
 137
 138
 139
 140
 141
 142
 143
 144
 145 **Fig. 1.** Latitude-longitude lattice (180 points)



146
 147
 148
 149
 150
 151
 152
 153
 154 **Fig. 2.** Fibonacci lattice (179 points)

148 2.3. Distortion measures

149 When we want to project a spherical surface onto a plane, distortions of several type will inevitably
 150 occur due to the fact that the sphere has a finite radius of curvature whereas the plane has an
 151 infinite one. This is also the case when the source reference surface is an ellipsoid. Distortions in
 152 the map projection are normally classified into linear distortions, areal distortions and angular
 153 distortions (Snyder, 1987). Some projections have been devised to avoid a particular type of
 154

Código de campo cambiado

Código de campo cambiado

Código de campo cambiado

155 distortion (e.g. so-called conformal projections avoid angular distortions and so-called equal-area
 156 projections avoid areal distortions), others have been designed for a compromise of approximate
 157 preservation of all properties (they yield tolerable errors in all linear, angular and areal measures),
 158 but none of them is completely free from distortions, so that instead of a perfect map projection for
 159 universal use we can find many different map projections each of them devised for a particular
 160 purpose and geographic area (Snyder, 1987; Canters and Declair, 1989).

161
 162 Conformal projections are currently used for producing official cartography such as national
 163 topographic maps. They preserve angles but suffer from different distortions in length and area. For
 164 a pair of infinitesimally close points i and j , we can define the linear distortion coefficient k_l as the
 165 ratio of the projected distance ds' to the original distance on the sphere or ellipsoid surface ds and
 166 obtain, after some derivations using differential geometry (Baselga, 2014), that
 167

$$168 \quad k_l = \frac{ds'}{ds} = \frac{\sqrt{(x_\varphi^2 + y_\varphi^2)d\varphi^2 + (x_\lambda^2 + y_\lambda^2)d\lambda^2 + 2(x_\varphi x_\lambda + y_\varphi y_\lambda)d\varphi d\lambda}}{\sqrt{\rho^2 d\varphi^2 + \nu^2 \cos^2 \varphi d\lambda^2}} \quad (5)$$

169 where $d\varphi$ and $d\lambda$ are the geographic coordinate differences between the infinitesimally close points
 170 so that $\varphi_j = \varphi_i + d\varphi$, $\lambda_j = \lambda_i + d\lambda$; x_φ , y_φ , x_λ and y_λ denote partial derivatives (evaluated all of them
 171 in point i) of the functions defining the map projection $x = x(\varphi, \lambda)$ and $y = y(\varphi, \lambda)$ respect to φ and
 172 λ ; and ρ and ν are the principal radii of curvature of the ellipsoid (R for the case of a sphere). The
 173 linear distortion coefficients for the particular cases $d\lambda = 0$ (distortion along meridian) and $d\varphi = 0$
 174 (distortion along parallel) are customary denoted by h and k respectively (Snyder, 1987). They can
 175 be easily computed as
 176

$$177 \quad h = k_{l_meridian} = k_l(d\lambda = 0) = \frac{\sqrt{x_\varphi^2 + y_\varphi^2}}{\rho} \quad (6)$$

$$178 \quad k = k_{l_parallel} = k_l(d\varphi = 0) = \frac{\sqrt{x_\lambda^2 + y_\lambda^2}}{\nu \cos \varphi} \quad (7)$$

180 It is well-known (Snyder, 1987) that in a conformal projection, given a point i , the linear distortion
 181 coefficient is independent of the direction ij (in contrast, for a non-conformal projection, length
 182 distortion is dependent on the coordinates of i as well as on the bearing from i to j).
 183

184 Therefore, for a point i in a conformal projection we have $k_l = h = k$ regardless of the situation of
 185 the nearby point j (the linear distortion coefficient is independent of direction). For a conformal
 186 projection it is also well-known (Snyder, 1987; Rajakovic and Lapaine, 2010) that the areal
 187 distortion coefficient k_2 – ratio of the projected differential area dS' to the original area on the
 188 ellipsoid or sphere dS – equals k_l squared
 189

$$190 \quad k_2 = \frac{dS'}{dS} = k_l^2 \quad (8)$$

191
 192 Other general measures of distortion include Tissot's ellipses (Snyder, 1987; Bauer-Marschallinger
 193 *et al.*, 2014) and derived measures (e.g. averaged ratio between complementary profiles, Yan *et al.*,
 194 2016). However, for the case of a conformal projection (no angular distortion, linear distortion k_l ,
 195 areal distortion $k_2 = k_l^2$ and Tissot's ellipses degenerated to circles of radius k_l) it seems sensible to
 196 study only k_l and, in particular, its typical deviation from the optimum value 1, as we will see next.
 197

198 Different optimization criteria have been proposed in the past, including the minimization of
 199 extreme linear distortions (Rajakovic and Lapaine, 2010) and minimization of several distortion
 200 estimators, such as the one introduced by Gilbert (1974) as
 201

Código de campo cambiado

Código de campo cambiado

Código de campo cambiado

Código de campo cambiado

$$E_G = \frac{(s - s')^2}{\sqrt{s^2 s'^2}} \quad (9)$$

where s and s' are the original distance on the sphere or ellipsoid surface and the projected distance, respectively, to be obtained and averaged over a sufficiently large number of randomly selected pairs of points in order to obtain an overall estimator of the distortion for the projection.

By virtue of Eq. (5) we can write

$$s' = \int_0^s k_l ds = k_l s \quad (10)$$

where in the last equality we have denoted by k_l the average linear distortion factor in the line (mean value theorem for integrals), so that substitution of Eq. (10) into Eq. (9) permits us to write

$$E_G = \frac{(s - k_l s)^2}{\sqrt{s^2 k_l^2 s^2}} = \frac{(1 - k_l)^2}{k_l} \quad (11)$$

In the same fashion, Peters (1975) proposed the use of his estimator

$$E_P = \frac{|s - s'|}{|s + s'|} \quad (12)$$

which, again, using Eq. (10) we can transform (Canters, 2002) into

$$E_P = \frac{|1 - k_l|}{|1 + k_l|} \quad (13)$$

Other classic distortion estimators include the integral evaluation of Airy (1861) and Jordan (1896)'s measures, given respectively by

$$e_{A_2} = \frac{1}{2} [(a_i - 1)^2 + (b_i - 1)^2] \quad (14)$$

being a_i and b_i the maximum and minimum linear distortion coefficients at the sample point, and

$$e_J = \frac{1}{2\pi} \int_0^{2\pi} (k_{li} - 1)^2 d\alpha \quad (15)$$

For conformal projections ($a_i = b_i = k_{li}$) these are respectively simplified to

$$e_{A_2} = (k_{li} - 1)^2 \quad (16)$$

and

$$e_J = (k_{li} - 1)^2 \quad (17)$$

In practice the mean distortion value can be calculated by dividing the region into n smaller areas, determining the value for the midpoint of each and computing the average value (Canters, 2002).

244 This discrete evaluation can be interpreted as an approximation, depending on the number and
 245 distribution of the points, to the computation by using integrals .

246 We can therefore characterize the overall linear distortion of a projection by computing the squared
 247 differences of the linear distortion factor k_I with respect to 1 – Airy and Jordan’s measures for the
 248 case of conformal projections – for a given (large) set of n sample points, obtaining thus a typical
 249 measure for the distortion Δk_I as
 250

$$251 \Delta k_I = \sqrt{\frac{1}{n} \sum_{i=1}^n (k_{I_i} - 1)^2} \quad (18)$$

253 The formula remembers that of the standard deviation only taking here 1 (the optimum value for k_I)
 254 instead of the average value of the sample. It will be referred to by the name of *typical distortion*
 255 and used as optimization function for the subsequent computations. It may be worth noting that a
 256 simple arithmetic mean of the differences of the linear distortion factor k_I with respect to 1 might
 257 not give meaningful information about the possible distortions since large positive values could be
 258 cancelled out by large negative values and is therefore not recommended. For the case of weighted
 259 latitude-longitude lattices – weight according to Eq. (1) – the corresponding function to be used is
 260

$$261 \Delta k_I = \sqrt{\frac{\sum_{i=1}^n (w_i k_{I_i} - 1)^2}{\sum_{i=1}^n w_i}} \quad (19)$$

263
 264

265 2.4. Optimization method

266 Map projections have some parameters (e.g. latitude of standard parallels) that have to be carefully
 267 selected in order to minimize the inevitable resulting distortions. The question of finding the best
 268 values for some parameters that yield the optimum value for a derived function is called an
 269 optimization problem. In general form, the optimization problem, i.e. the determination of the
 270 optimum vector \mathbf{x} within a prescribed search domain D that makes the objective function f reach
 271 the global minimum, is formulated as
 272

$$273 \begin{cases} \min f(\mathbf{x}) \\ \text{subject to } \mathbf{x} \in D \end{cases} \quad (20)$$

274
 275 In our present case, the so-called objective function f will be Eq. (18) for some variables to
 276 optimize \mathbf{x} (e.g. latitude of standard parallels) in the desired domain D (defined by some boundaries
 277 for the area of interest or, simply, the entire Earth).

278
 279 One of the most successful methods devised for solving optimization problems is the Simulated
 280 Annealing (SA) method, originally developed by Metropolis et al. (1953), which emulates the
 281 process of crystalline network self-construction. It has been extensively used in the last years,
 282 particularly in the field of geosciences (e.g. Berné and Baselga, 2004; Santé-Riveira et al., 2008;
 283 Baselga, 2011; Sharma, 2012; Chimi-Chiadjeu et al., 2013; and Soltani-Mohammadi et al., 2016).
 284 We will not delve into the many technicalities of the method and simply refer to specific
 285 publications (e.g. van Laarhoven and Aarts, 1987; Pardalos and Romeijn, 2002).
 286

287 We will compare our results with alternative procedures for defining the latitudes of standard
 288 parallels in conic projections, in particular with the 1/6 rule of thumb consisting in placing the
 289 standard parallels at 1/6th of the maximum and minimum latitudes (e.g. Fenna, 2007; and Jenny,

Código de campo cambiado

Código de campo cambiado

290 2012) and the work by Savric and Jenny (2016), which gives polynomial models to determine
 291 standard parallels for three conic projections given the spatial extent of the desired mapped area.
 292

293 3. Evaluation of map distortions

294
 295 We analyze here the Lambert Conformal Conic projection that was first recommended by
 296 EuroGeographics (Annoni *et al.*, 2003) and then officially adopted by INSPIRE D2.8.I.1 (2014) as
 297 the standard for conformal mapping in Europe. This projection is also the same (including standard
 298 parallels) known as EPSG3034 in the database initially developed by the European Petroleum
 299 Survey Group – and currently maintained by the International Association of Oil & Gas Producers
 300 (OGP) – which has become a standard for the definition of coordinate reference systems
 301 (International Organization for Standardization, 2007).
 302

303 This projection is to be used in Europe along with the official reference system ETRS89 with the
 304 defining parameters given in Table 1 (Annoni *et al.*, 2003).
 305

306 **Table 1**

307 Defining parameters for Lambert Conformal Conic projection for Europe in ETRS89 system and bounding
 308 box as given in (Annoni *et al.*, 2003).
 309

Parameter	Value
lower standard parallel latitude φ_l	35° N
upper standard parallel latitude φ_u	65° N
latitude of (false) grid origin φ_b	52° N
longitude of (false) grid origin λ_0	10° E
False northing N_0	2800000
False easting E_0	4000000
Maximum latitude φ_{max}	71° N
Minimum latitude φ_{min}	27° N
Maximum longitude λ_{max}	45° E
Minimum longitude λ_{min}	30° W

310
 311 Defining a and b as the major and minor semiaxes of the ellipsoid (ellipsoid GRS80 for the case of
 312 reference system ETRS89), f ellipsoid flattening, and e its first eccentricity, we can subsequently
 313 compute for a point to be projected of latitude φ and longitude λ (Annoni *et al.*, 2003):
 314

$$315 \quad Q_l = \frac{1}{2} \left[\ln \left(\frac{1 + \sin \varphi_l}{1 - \sin \varphi_l} \right) - e \ln \left(\frac{1 + e \sin \varphi_l}{1 - e \sin \varphi_l} \right) \right] \quad (21)$$

$$316 \quad W_l = (1 - e^2 \sin^2 \varphi_l)^{1/2} \quad (22)$$

$$317 \quad Q_u = \frac{1}{2} \left[\ln \left(\frac{1 + \sin \varphi_u}{1 - \sin \varphi_u} \right) - e \ln \left(\frac{1 + e \sin \varphi_u}{1 - e \sin \varphi_u} \right) \right] \quad (23)$$

$$318 \quad W_u = (1 - e^2 \sin^2 \varphi_u)^{1/2} \quad (24)$$

$$319 \quad \sin \varphi_0 = \frac{\ln \left(\frac{W_u \cos \varphi_l}{W_l \cos \varphi_u} \right)}{Q_u - Q_l} \quad (25)$$

$$320 \quad K = \frac{a \cos \varphi_l \exp(Q_l \sin \varphi_0)}{W_l \sin \varphi_0} \quad (26)$$

321

Código de campo cambiado

Código de campo cambiado

Código de campo cambiado

Código de campo cambiado

Código de campo cambiado

Código de campo cambiado

Código de campo cambiado

Código de campo cambiado

Código de campo cambiado

Código de campo cambiado

322
323
324
325
326
327
328
329
330
331
332
333
334
335
336
337
338
339
340
341
342
343
344
345
346
347
348
349
350
351
352
353
354
355
356
357
358
359
360
361
362
363
364
365
366
367
368

$$Q = \frac{1}{2} \left[\ln \left(\frac{1 + \sin \varphi}{1 - \sin \varphi} \right) - e \ln \left(\frac{1 + e \sin \varphi}{1 - e \sin \varphi} \right) \right] \quad (27)$$

$$R = \frac{K}{\exp(Q \sin \varphi_0)} \quad (28)$$

$$k = (1 - e^2 \sin^2 \varphi)^{1/2} \frac{R \sin \varphi_0}{a \cos \varphi} \quad (29)$$

After computation of all the auxiliary quantities we arrive at the linear distortion coefficient k . (Note: remember the fact that $k_l = h = k$ with Eqs. (5)-(7) since it is a conformal projection).

Now Annoni *et al.* (2003) give maximum and minimum linear distortion coefficients in the given boundaries, respectively 43704 ppm and -34378 ppm, but do not provide a figure for the *typical distortion* that could be expected. We will now use Eqs. (21)-(29) to evaluate the typical distortion – Eq. (18) – that is produced in this map projection for the assumed bounding box using different lattices (of latitude-longitude and Fibonacci types).

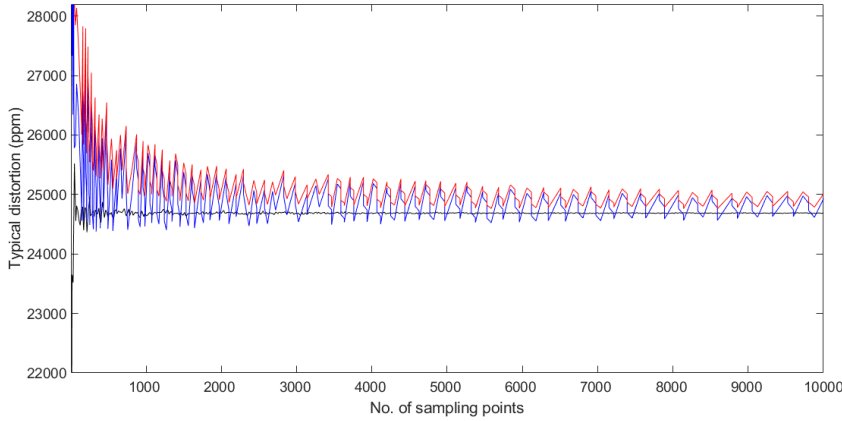
With the use of latitude-longitude lattices we find that we need a very large number of sampling points in the area (small step size δ) to obtain a value for Eq. (18) that is somewhat stable (i.e. that does not depend significantly on the number of sampling points), and even then the value keeps oscillating a bit.

When we use weighted latitude-longitude lattices we find more stable results and a significantly quicker convergence. However, both unweighted and weighted latitude-longitude lattices are clearly outperformed by the use of Fibonacci lattices, which yield a very quick and stable convergence to the final value $\Delta k_l = 0.024687 = 24687$ ppm Table 2 and Fig. 3 summarize these results.

Table 2
Intervals of typical distortion values Δk_l in terms of different number of lattice points in the area under study for three types of lattices: latitude-longitude, weighted latitude-longitude and Fibonacci.

Δk_l value (ppm)	Lat-lon lattice: No. of points	Weighted lat-lon lattice: No. of points	Fibonacci lattice: No. of points
24687 ± 100 ppm	~300000	~83000	~430
24687 ± 10 ppm	-	~1000000	~6800
24687 ± 1 ppm	-	-	~27000

We stopped the computations when lattices reached a few million sampling points due to their high computational cost (several minutes in a standard personal computer) therefore some cases in the table could not even be computed. We can see that by using unweighted latitude-longitude lattices we have trouble to find a solution value that is stable to the level of 100 ppm. In Fig. 3 we can see that the main reason is that the estimate we get for Δk_l is biased due to the unnecessary higher density of sampling points at higher latitudes. The computation is improved by the use of weighted latitude-longitude lattices, by which we can reach with effort a solution within 10 ppm. By contrast, the use of Fibonacci lattices permits us to obtain a quick convergence so that a solution within 1 ppm can easily be obtained by using around 27000 sampling points only.



386 **Fig. 3.** Typical distortion values Δk_l in terms of different number of lattice points (only up to 10000 points
 387 shown here) using three types of lattices: latitude-longitude (red), weighted latitude-longitude (blue) and
 388 Fibonacci (black).

389 We have shown that the typical distortion to be expected for the Lambert Conformal Conic
 390 projection using the parameters and bounding box defined for Europe, Table 1, is 24687 ppm and
 391 that it can be easily obtained with a small number of sampling points if we use a Fibonacci lattice
 392
 393

394 4. Optimization of map projections

395 We examine now whether the typical distortion value for the Lambert Conformal Conic projection
 396 can be improved by the use of different standard parallels than the ones conventionally used in
 397 Europe as well as compute the best ones for using the projection in Spain.
 398
 399

400 The following new procedure optimizes a map projection by computing the standard parallels that
 401 minimize the typical distortion of the desired area. We understand the question as a global
 402 optimization problem in which the typical distortion Δk_l has to be minimized for a sufficient and
 403 efficient lattice of the area under study being the standard parallel latitudes the variables to
 404 optimize.
 405
 406

407 4.1. Optimization of Lambert Conformal Conic projection for Europe

408 We see now how the standard parallels included as the defining variables of the Lambert
 409 Conformal Conic projection for Europe, Table 1, can be optimized so that the typical distortion of
 410 the area, Eq. (18) using Eq. (29) as the particular linear distortion coefficient, can be minimized.
 411 We will use here the simulated annealing method as the optimization method (eventually the final
 412 results should be the same by means of other competent optimization method) and a Fibonacci
 413 lattice as efficient sampling set, once we have seen its excellent performance in the previous
 414 section.
 415
 416

417 We take into account the specific search domain, i.e. geographic boundaries in Table 1 (44°-wide in
 418 latitude and 75°-wide in longitude), use as the initial solution for the vector to optimize e.g. $\mathbf{x}_0 =$
 419 $(\varphi_{l0}, \varphi_{\lambda 0}) = (35^\circ, 65^\circ)$, i.e. the values given in Table 1, and define the corresponding search domains
 420 as $\varphi_l \in [\varphi_{min}, (\varphi_{min} + \varphi_{max})/2]$ and $\varphi_\lambda \in [(\varphi_{min} + \varphi_{max})/2, \varphi_{max}]$. Given the results obtained in the
 421 previous section and wanting to have typical distortions computed to some 1 ppm, we decide to use
 422 a Fibonacci lattice with 28161 lattice points in the area. The algorithm converges to the optimum
 423 solution after some 100 to 150 iterations only (Figs. 4 and 5).
 424

425
426
427
428
429
430
431
432
433
434
435
436
437
438
439
440
441
442
443
444
445
446
447
448
449
450
451
452
453
454
455
456
457
458
459
460
461
462
463
464
465
466
467
468
469
470
471
472
473
474
475
476
477
478
479
480
481

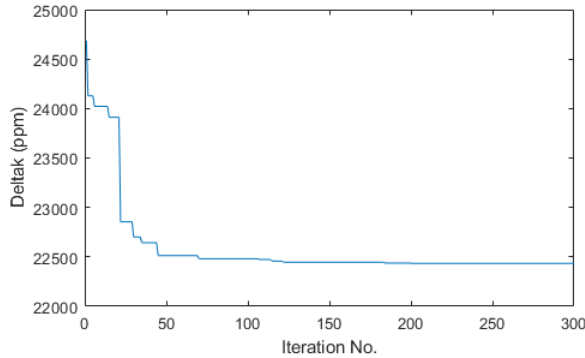


Fig. 4. Evolution of computed best value Δk_I (ETRS89-Lambert Conformal Conic projection for Europe).

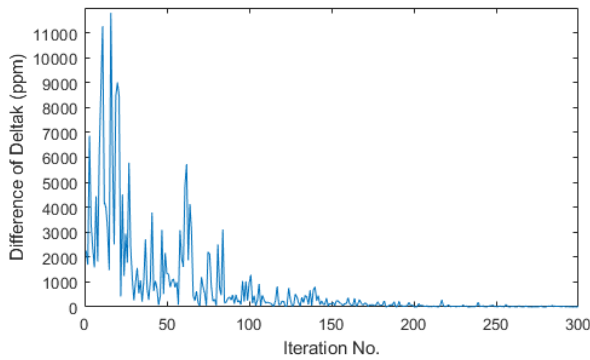


Fig. 5. Differences between current iteration value and final best value for Δk_I (ETRS89-Lambert Conformal Conic projection for Europe).

We obtain a global optimum at $\varphi = 36.06^\circ$, $\varphi_u = 61.54^\circ$ with $\Delta k_I = 22434$ ppm. We obtain an almost indistinguishable result if we round to the next half-integer the standard parallel latitudes: $\varphi = 36^\circ$, $\varphi_u = 61.5^\circ$ with $\Delta k_I = 22435$ ppm.

These standard parallel latitudes are not very different from the ones customary used ($\varphi = 35^\circ$, $\varphi_u = 65^\circ$). However, we see a considerable decrease in the typical distortion of around 10% (from 24687 to 22435 ppm). In Table 3 we show the different results we obtain for the typical distortion Δk_I also using the 1/6 rule of thumb and Savric and Jenny (2016) method. We also show other measures: Gilbert and Peters estimators, as well as average, maximum and minimum values of the linear distortion coefficient. It is worth mentioning that Savric and Jenny (2016)'s method was designed to optimize the standard parallels on the sphere, while we are using here ellipsoidal equations for the Lambert conformal conic projection. Savric and Jenny's method also assumes symmetry along the central meridian for the area of interest; therefore, we had to set symmetrical limits in longitude for the computation of optimum standard parallels with it, although the final evaluation of typical distortion was done for the non-symmetrical true area of interest.

482 **Table 3**
483 Different proposals for lower and upper standard parallels (φ_l and φ_u) along with their corresponding typical
484 distortion (Δk_l), Gilbert and Peters estimators (E_G and E_P) and average, maximum and minimum values of
485 linear distortion coefficient (k_{lavg} , k_{lmax} and k_{lmin}) for Lambert Conformal Conic projection for Europe.
486

Source	φ_l (°)	φ_u (°)	Δk_l (ppm)	E_G (ppm)	E_P (ppm)	k_{lavg} (ppm)	k_{lmax} (ppm)	k_{lmin} (ppm)
INSPIRE D2.8.I.1 (2014) / Annoni et al.(2003) / EPSG3034	35	65	24687	617	11094	-9147	43704	-34378
1/6 rule of thumb (Jenny 2012, Fenna 2007)	34.33	63.67	23874	576	10673	-8518	54954	-32827
Savric and Jenny (2016)	37.55	58.68	23925	551	9064	7012	84836	-16988
Present method	36.06	61.54	22434	496	9514	-496	67600	-24733
Present method rounded to nearest half-integer	36	61.5	22435	496	9512	-566	68040	-24771

487
488 The standard parallels determined by our method clearly reduce the typical distortion in the area as
489 compared with the parallels given by EuroGeographics and the INSPIRE directive (10% distortion
490 reduction), 1/6 rule of thumb (6% distortion reduction), and Savric and Jenny (2016) polynomials
491 (6% distortion reduction). Our method yields also the best solution in terms of Gilbert estimator
492 and average distortion in the area, though it gives a second-best solution for Peters estimator just
493 after Savric and Jenny's method, which, in turn, yields the highest distortion value in the area
494 among all the different solutions. Having sought a solution that minimizes the typical distortion,
495 Eq. (18), entailing minimization of Airy and Jordan estimators, we find a result that is also better
496 than the alternative methods regarding Gilbert estimator and average distortion. It could be argued
497 that our solution yields suboptimal values for other measures; however, considering that no single
498 solution minimizes all values, the definition of the best projection in terms of the one minimizing
499 the typical distortion as well as being the best in terms of other important distortion measures
500 (average distortion and Gilbert estimator) seems a judicious one.
501
502

503 4.2. Optimization of Lambert Conformal Conic projection for Spain

504
505 We can use the same method to optimize the standard parallels to be used in the official Lambert
506 Conformal Conic projection for Spain. A decree from the Gobierno del Estado Español (2007)
507 commands that the ETRS89 reference system and the Lambert Conformal Conic projection be
508 officially adopted for land representation at mapping scales of 1:500.000 or lower, without fixing,
509 however, the particular latitudes to be used for the standard parallels. We use the same approach,
510 simulated annealing as optimization method and a Fibonacci lattice for efficient sampling of the
511 mapped area. As the problem geographic boundaries we use now those from EPSG3429 type area
512 for "Spain mainland and Balearic Islands", namely $\varphi_{min} = 35.26^\circ$ N, $\varphi_{max} = 43.82^\circ$ N, $\lambda_{min} = 9.37^\circ$ W
513 and $\lambda_{max} = 4.39^\circ$ E. We start with some arbitrary values in the search domain as initial solution e.g.
514 $\mathbf{x}_0 = (\varphi_0, \varphi_{u0}) = (\varphi_{min}, \varphi_{max})$; the final solution being independent from this choice. The algorithm
515 quickly converges to the optimum solution after a few iterations (Figs. 6 and 7).
516
517
518
519
520
521
522
523
524
525

526
 527
 528
 529
 530
 531
 532
 533
 534
 535
 536
 537
 538
 539
 540
 541
 542
 543
 544
 545
 546
 547
 548
 549
 550
 551
 552
 553
 554
 555
 556
 557
 558
 559
 560
 561
 562
 563
 564
 565
 566
 567
 568
 569
 570
 571
 572
 573
 574
 575
 576
 577
 578
 579
 580
 581
 582
 583

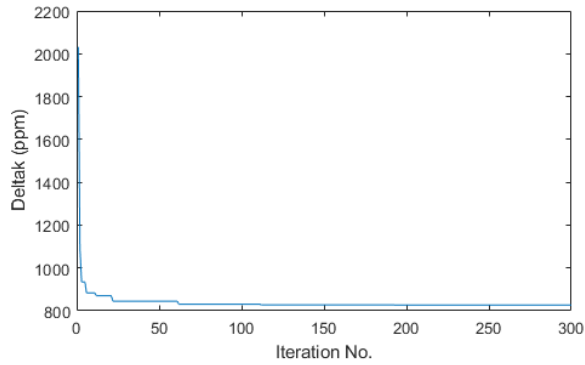


Fig. 6. Evolution of computed best value Δk_l (ETRS89-Lambert Conformal Conic projection for Spain).

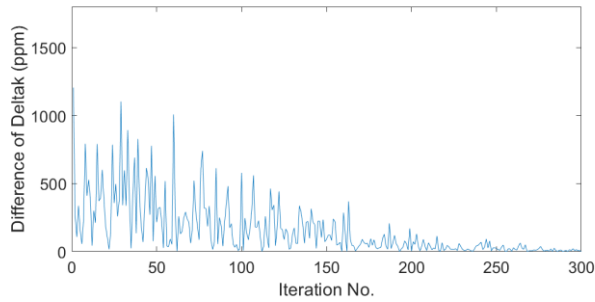


Fig. 7. Differences between current iteration value and final best value for Δk_l (ETRS89-Lambert Conformal Conic projection for Spain).

We obtain a global optimum at $\varphi_l = 37.07^\circ$, $\varphi_u = 42.00^\circ$ with $\Delta k_l = 827$ ppm and a practically indistinguishable result if we round to the next integer these standard parallel latitudes: $\varphi_l = 37^\circ$, $\varphi_u = 42^\circ$ with $\Delta k_l = 828$ ppm.

We can see in Table 4 that there is a 1.5% distortion reduction for our proposal with respect to that of Savric and Jenny (2016) and a 7% distortion reduction with respect to that of the 1/6 rule of thumb. Similarly to the case of Europe (Table 3), our method gives also the best solution in terms of Gilbert estimator and average distortion in the area, and a second-best for Peters estimator right after Savric and Jenny's method, which, in turn, yields the highest distortion value in the area among all different solutions.

584 **Table 4**
585 Different proposals for lower and upper standard parallels (φ_l and φ_u) along with their corresponding typical
586 distortions (Δk_l), Gilbert and Peters estimators (E_G and E_P) and average, maximum and minimum values of
587 linear distortion coefficient (k_{lavg} , k_{lmax} and k_{lmin}) for Lambert Conformal Conic projection for Spain.
588

Source	φ_l (°)	φ_u (°)	Δk_l (ppm)	E_G (ppm)	E_P (ppm)	k_{lavg} (ppm)	k_{lmax} (ppm)	k_{lmin} (ppm)
1/6 rule of thumb (Jenny 2012, Fenna 2007)	36.69	42.39	883	0.78	394	-311	1581	-1235
Savric and Jenny (2016)	37.29	41.82	840	0.70	348	145	2027	-779
Present method	37.07	42.00	827	0.68	356	2	1908	-922
Present method rounded to nearest integer	37	42	828	0.68	358	-25	1928	-948

589

590 5. Conclusions

591 In the present paper we have shown the clear advantages in performance of Fibonacci lattices with
592 respect to the standards latitude-longitude lattices for numerical evaluation of map distortions.
593

594 We have computed the typical distortion for the Lambert Conformal Conic projection with their
595 currently defined parameters and geographic boundaries for Europe, adopted as standard by
596 INSPIRE, resulting in 24687 ppm. Further, we have optimized the defining parameters of this
597 projection so that the typical distortion for the area of interest (Europe) is reduced a 10%. We
598 therefore recommend a change in the definition of standard parallel latitudes for the Lambert
599 Conformal Conic projection in Europe so that lower and upper standard parallels be set to 36° and
600 61.5°, respectively.
601

602 We also apply the optimization procedure to the determination of the best standard parallels for
603 using the Lambert Conformal Conic projection in Spain, whose values remained unspecified by the
604 National decree that commanded its official adoption. We obtain a best pair of standard parallels of
605 latitudes 37° and 42° for which the typical distortion results in 828 ppm.
606

607 Acknowledgements

608
609 The author sincerely appreciates the comments, suggestions and computation double checking by
610 the anonymous reviewers that helped improve the manuscript.
611

612 References

- 613
614 Airy, G. B., 1861. Explanation of a projection by balance of errors for maps applying to a very large extent of
615 the Earth's surface, and comparison of this projection with other projections. London, Edinburgh and Dublin
616 Philosophical Magazine, 4th ser., 22: 409–421.
- 617 Annoni, A., Luzet, C., Gubler, E. and Ihde, J., 2003. Map Projections for Europe. European Commission
618 Joint Research Centre, Ispra, Italy. EUR 20120 EN.
- 619 Baselga, S., 2011. Second Order Design of Geodetic Networks by the Simulated Annealing Method. Journal
620 of Surveying Engineering, 137(4): 167–173.
- 621 Baselga, S., 2014. Fundamentos de Cartografía Matemática. 2nd ed. Universitat Politècnica de València,
622 València.
- 623 Bauer-Marschallinger, B., Sabel, D. and Wagner, W., 2014. Optimisation of global grids for high-resolution
624 remote sensing data. Computers & Geosciences, 72: 84–93.
- 625 Berné, J.L. and Baselga, S., 2004. First-Order Design of Geodetic Networks using the Simulated Annealing
626 Method. Journal of Geodesy, 78(1): 47–54.

627 Canters, F., 2002. *Small-scale Map Projection Design*. Taylor & Francis, London,

628 Canters, F., and Declair, H., 1989. *The World in Perspective: A Directory of World Map Projections*. John
629 Wiley and Sons, Chichester.

630 Chimi-Chiadjeu, O., Vannier, E., Dusséaux, R., Le Hégarat-Masclé, S. and Taconet, O., 2013. Using
631 simulated annealing algorithm to move clod boundaries on seedbed digital elevation model. *Computers &*
632 *Geosciences*, 57: 68–76.

633 Conway, J. H. and Sloane, N. J. A., 1998. *Sphere packings, lattices and groups*. 3rd edn. Springer, New
634 York.

635 Crăciun, C., 2014. Homogeneity and EPR metrics for assessment of regular grids used in CW EPR powder
636 simulations. *Journal of Magnetic Resonance*, 245: 63–78.

637 Fenna, D., 2007. *Cartographic Science: A Compendium of Map Projections, with Derivations*. CRC Press,
638 Taylor & Francis Group, Boca Raton.

639 Gilbert, E. N., 1974. Distortion in maps. *Society for Industrial and Applied Mathematics Review*, 16: 47–62.

640 Gobierno del Estado Español, 2007. Gobierno del Estado Español, Real Decreto 1071/2007, de 27 de julio,
641 por el que se regula el sistema geodésico de referencia oficial en España. *Boletín Oficial del Estado*, 207:
642 35986–35989.

643 González, A., 2010. Measurement of Areas on a Sphere Using Fibonacci and Latitude–Longitude Lattices.
644 *Mathematical Geosciences*, 42: 49–64.

645 INSPIRE D2.8.I.1, 2014. *Data Specification on Coordinate Reference Systems – Technical Guidelines*

646 International Organization for Standardization, 2007. *Geographic information – Spatial referencing by*
647 *coordinates (ISO Standard No. 19111)*. Retrieved from <https://www.iso.org/standard/41126.html>

648 Jenny, B., 2012. Adaptive composite map projections. *IEEE Trans. Vis. Comput. Graph.*, 18(12): 2575–
649 2582.

650 Jordan, W., 1896. Der mittlere Verzerrungsfehler. *Zeitschrift für Vermessungswesen*, 25: 249–252.

651 Koshy, T., 2001. *Fibonacci and Lucas Numbers with Applications*. Wiley-Interscience, New York.

652 Marques, R., Bouville, C., Ribardiere, M., Santos, L. P. and Bouatouch, K., 2013. Spherical Fibonacci Point
653 Sets for Illumination Integrals. *Computer Graphics Forum*, 32(8): 134–143.

654 Metropolis, N., Rosenbluth, M., Rosenbluth, A., Teller, A., and Teller, E., 1953. Equation of state
655 calculations by fast computing machines. *J. Chem. Phys.*, 21(6): 1087–1092.

656 Monechi, B., Servedio, V. D. P. and Loreto, V., 2015. Congestion Transition in Air Traffic Networks. *PLoS*
657 *ONE*, 10(5): e0125546. doi:10.1371/journal.pone.0125546

658 Pardalos, P. M., and Romeijn, H. E., eds., 2002. *Handbook of global optimization, Vol 1&2*, Kluwer
659 Academic, Dordrecht.

660 Peters, A. B., 1975. Wie man unsere Weltkarten der Erde ähnlicher machen kann. *Kartographische*
661 *Nachrichten*, 25: 173–183.

662 Purser, R. J., 1999. Non-standard Grids. *Proceedings of the ECMWF Seminar on Recent Developments in*
663 *Numerical Methods for Atmospheric Modelling*, p. 44-72, 7–11 September 1998.

664 Rajakovic, M., and Lapaine, M., 2010. The Best Conic Conformal Map Projection for the Territory of
665 Croatia. *Kartografija i Geoinformacije*, 9(14): 24–44.

666 Santé-Riveira, I., Boullón-Magán, M., Crecente-Maseda, R. and Miranda-Barrós, D., 2008. Algorithm based
667 on simulated annealing for land-use allocation. *Computers & Geosciences*, 34: 259–268.

668 Šavrič, B. and Jenny, B., 2016. Automating the selection of standard parallels for conic map projections.
669 *Comput. Geosci.* 90: 202–212.

670 Sharma, S. P., 2012. VFSARES—a very fast simulated annealing FORTRAN program for interpretation of
671 1-D DC resistivity sounding data from various electrode arrays. *Computers & Geosciences*, 42: 177–188.

672 Snyder, J. P., 1987. *Map Projections: A Working Manual*. US Geological Survey, Washington, DC.

673 Soltani-Mohammadi, S., Safa, M. and Mokhtari, H., 2016. Comparison of particle swarm optimization and
674 simulated annealing for locating additional boreholes considering combined variance minimization.
675 *Computers & Geosciences*, 95: 146–155.

676 Sparrow, K. H. and Mercer, A. E., 2016. Predictability of US tornado outbreak seasons using ENSO and
677 northern hemisphere geopotential height variability. *Geoscience Frontiers*, 7(1): 21–31.

678 Swinbank, R. and Purser, R. J., 2006. Fibonacci grids: A novel approach to global modelling. *Quarterly*
679 *Journal of the Royal Meteorological Society*, 132: 1769–1793.

680 van Laarhoven, P. J. M. and Aarts, E. H. L., 1987. *Simulated annealing: theory and applications*, Reidel,
681 Dordrecht.

682 Yan, J., Song, X., Gong, G., 2016. Averaged ratio between complementary profiles for evaluating shape
683 distortions of map projections and spherical hierarchical tessellations. *Computers & Geosciences*, 87: 41–55.

684